RSC Advances

PAPER

View Article Online
View Journal | View Issue

Cite this: *RSC Adv.*, 2025, **15**, 37979

Influence of pH and sulfate concentration on hydrous ferric arsenate transformation behavior and As(v) mobilization

Xuedi Wang,[a] Rui Su, *[a] Miao Xu,[a] Yuyin Ma,[b] Yanjiao Gao[a] and Xu Ma*[b]

Received 17th July 2025
Accepted 3rd October 2025

DOI: 10.1039/d5ra05160f

rsc.li/rsc-advances

This study investigates the effect of various SO_4^{2-} concentrations (0, 50, and 100 mM) on the phase transformation of hydrous ferric arsenate (HFA) and partitioning behaviors of As(v), Fe(iii), and SO_4^{2-} under ambient (25 °C, 15 d) and subsequent elevated temperature (80 °C, 35 d) conditions. The results revealed that the primary factor controlling the transformation of HFA into crystalline scorodite was the pH, whereas the SO_4^{2-} concentration played a secondary, pH-dependent role. More specifically, at pH 4 and under ambient temperature, SO_4^{2-} enhanced the release of As(v) and Fe(iii) into the solution. By contrast, at pH 6 and 8, SO_4^{2-} promoted the formation of basic ferric arsenate sulfate, which immobilized As(v), and later dissolved upon heating. SO_4^{2-} incorporation into the solid phase occurred across all pH levels and was enhanced at higher concentrations and temperatures. Thus, SO_4^{2-} modulates As(v) mobility *via* structural incorporation and ion competition, with distinct behaviors at acidic *versus* circumneutral pH. These findings offer guidance for risk assessment and design of sulfate-rich, mining-impacted remediation systems.

1. Introduction

Arsenic (As) is a toxic metalloid,[1,2] which often co-exists with iron (Fe) and sulfur (S) in alkali and precious metal ores in the form of Fe–As–S bearing minerals such as pyrite and arsenopyrite. The abiotic and biotic dissolution and oxidation of such original minerals can release significant amounts of As(v), Fe(iii), and SO_4^{2-} into natural and anthropogenic environments, such as acid mine drainage (AMD),[3–5] geothermal springs,[6] and contaminated soils,[7,8] thereby posing global environmental and health risks.[3,4,9–13]

In aerobic surface environments with abundant Fe(iii), hydrous ferric arsenate (HFA) serves as a critical sink for As(v) under acidic to circumneutral pH conditions.[14–17] HFA primarily forms through rapid Fe(iii)–As(v) co-precipitation or *via* transformation of adsorbed-As(v) on iron (oxyhydr)oxide surfaces such as ferrihydrite and goethite.[9,18] Natural analogues of HFA compounds have been found in diverse environments, including sea-floor hydrothermal vents,[19] microbial mats at geothermal springs,[6] and in mine-impacted environments,[10,20] underscoring the relevance of HFA in natural and contaminated settings. Hence, HFA formation is crucial for As scavenging from aqueous solutions.

Owing to its amorphous nature, the pH and presence of co-existing ions significantly affect the precipitation and dissolution of HFA.[11,21–23] Within the pH range of 3–5, HFA exhibits relatively low solubility, often releasing between 5–50 mg L^{-1} of As(v).[24,25] However, its stability decreases markedly outside this range—below pH 3, proton-promoted dissolution increases the release of arsenic, whereas above the pH range of ~5–6, HFA becomes thermodynamically unstable and tends to transform into more crystalline iron oxides (such as ferrihydrite, goethite, or hematite), resulting in the release of previously sequestered As(v) back into the solution.[9,18,26,27] In addition to pH, the co-existing sulfate (SO_4^{2-}) can significantly alter the precipitation and dissolution behavior of HFA, specifically in strongly acidic systems (pH < 2). This effect may be attributed to the similar geometries and charges of the $HAsO_4^{2-}$ and SO_4^{2-}, which allow the isomorphic substitution of $HAsO_4^{2-}$ with SO_4^{2-} in HFA. Consequently, this process reduces As(v) precipitation and promotes HFA dissolution.[10,28,29]

In waterlogged mine sites, fluctuating pH values and SO_4^{2-} inputs from sulfide oxidation–dissolution can significantly alter the environmental behavior of HFA.[18,30,31] Previous studies that examined the effects of SO_4^{2-} under strongly acidic conditions (pH < 2) reported that SO_4^{2-} inhibits As(v)–Fe(iii) precipitation *via* Fe(iii)–SO_4^{2-} complexation while simultaneously enhancing HFA solubility by destabilizing the Fe(iii)–As(v) bonds.[31–34] However, the impact of the SO_4^{2-} input on the mobility and transformation of HFA at environmentally relevant pH levels (pH 4–8) may differ substantially from that observed at pH < 2.[26,32,33] In systems experiencing pH fluctuations, such as AMD-

[a]*College of Civil Engineering and Architecture, Liaoning University of Technology, Jinzhou, 121001, China. E-mail: surui@lnut.edu.cn*

[b]*College of Environment and Resources, Dalian Minzu University, Dalian, 116600, China. E-mail: maxu@dlnu.edu.cn*

impacted sites, the interactions between SO_4^{2-} and HFA at pH 4–8 are yet to be explored. Similarly, the effects of this anion on HFA stability and the associated As(v) mobility under near-neutral pH conditions are yet to be investigated, thereby limiting our understanding of As(v) cycling in such settings. Under these conditions, SO_4^{2-} may either trigger the transformation of HFA to secondary ferrihydrite or stabilize HFA through ion competition, leading to subsequent As(v) release. However, current models lack data related to the SO_4^{2-}-driven behavior of HFA in this pH range, thereby limiting the predictive capability for As(v) mobility in dynamic environments.

Thus, this study systematically examines the mechanisms by which SO_4^{2-} modulates the HFA transformation and As(v) mobility across the pH range of 4–8, under ambient and subsequent elevated-temperature conditions, to elucidate the dual roles of SO_4^{2-} in As(v) sequestration and remobilization. The solute SO_4^{2-} concentrations (0, 50, and 100 mM) and pH values (4, 6, and 8) considered in this study are representative of those found in AMD, hydrometallurgical tailings, and As-bearing effluents. The resulting solid-phase transformations are characterized using X-ray diffractometry (XRD), Raman spectroscopy, Fourier-transform infrared (FTIR) spectroscopy, and X-ray photoelectron spectroscopy (XPS). Additionally, the aqueous As(v) and Fe concentrations are monitored to assess any changes in solubility.

2. Experimental

2.1 Synthesis of hydrous ferric arsenate (HFA)

HFA was synthesized using a previously reported method.[32] Specifically, an As(v) stock solution (200 ml, 0.2 mol L^{-1}) was prepared using As_2O_5 and mixed with an Fe(III) solution (200 ml 0.2 mol L^{-1}) derived from $Fe(NO_3)_3 \cdot 9H_2O$, while maintaining a molar Fe(III)/As(v) ratio of 1 : 1. Next, the pH of the mixed solution was adjusted to 1.8 with HCl or NaOH (0.1 mol L^{-1}) to form the HFA precipitate. Subsequently, three suspensions were thus prepared, and their pH was adjusted to 4, 6, or 8, respectively, using HCl or NaOH (0.1 mol L^{-1}) and maintained for 5 d to stabilize the HFA precipitate.

2.2 Sulfate amendment and transformation experiments

To evaluate the effect of SO_4^{2-} on HFA transformation, SO_4^{2-} was introduced into the pre-stabilized HFA suspensions to achieve final concentrations of 0, 50, and 100 mM. The suspensions were continuously stirred and maintained at 25 ± 1 °C. Aliquots (5 ml) of the suspensions were then collected at predetermined time intervals (*i.e.*, 0, 1, 3, 5, 7, 10, and 15 d). After 15 d, the suspensions were transferred to an incubator for thermal ageing at 80 °C. Additional samples were then collected on days 16, 17, 20, 23, 25, 30, 35, 40, 45, and 50.

Throughout these experiments, pH was maintained at the target values (4, 6, and 8, respectively) using dilute NaOH or HCl solutions, as required. pH was adjusted by micro-titration with 0.01–0.1 mol per L HCl/NaOH (no buffer to avoid competing anions) and measured at each sampling. The background ionic strength was set to 10 mM $NaNO_3$. If the drift exceeded ± 0.05 pH units, pH was re-adjusted; the time course of pH is shown in Fig. S1. All experiments were performed in triplicate ($n = 3$), and data are reported as mean ± standard deviation; error bars in figures denote one standard deviation. All collected samples were filtered through 0.22 μm membranes. The solid products were washed with HCl or NaOH solutions adjusted to the corresponding pH values, freeze-dried at −50 °C, and stored in a desiccator.

2.3 Elemental analysis

The solid samples were digested using a 6 mol per L HCl solution to determine the concentrations of Fe(III), As(v), and SO_4^{2-} in the solid phases. The concentrations of As(v) within the solution was determined utilizing an atomic fluorescence spectrometer (AFS, Haiguang, China), and the concentrations of Fe(III) was determined utilizing flame atomic absorption spectroscopy (FAAS, Varian, USA). The limits of detection for the AFS and FAAS methods were approximately 0.01 μg L^{-1} and 10 μg L^{-1}, respectively. The concentration of SO_4^{2-} was determined by ion chromatography (IC, Metrohm 881, Switzerland) with a detection limit of 10 μg L^{-1} and relative uncertainty of ±5%.[35]

2.4 Solid characterization

Solid-phase mineralogical and structural analyses were performed *via* powder XRD, FTIR, Raman, and XPS. Detailed instrumental parameters and data processing methods are given in the SI.

3. Results and discussion

3.1 Aqueous phase dynamics of SO_4^{2-}, As(v), and Fe(III)

To assess the effects of the SO_4^{2-} concentration on HFA transformation, temporal changes in aqueous SO_4^{2-} concentrations were initially monitored over a 50 d period. Specifically, this experiment comprised an initial 15 d reaction at ambient temperature (25 °C), followed by a 35 d thermal aging phase at 80 °C. As shown in Fig. 1 and Table S1, the concentration of SO_4^{2-} remains relatively stable during the ambient phase, regardless of the pH (4, 6, or 8) or the initial SO_4^{2-} concentration (0, 50, or 100 mM), thereby indicating minimal early incorporation of this anion into the solid phase. This observation suggests that ambient temperature has negligible effect on the redistribution of SO_4^{2-} between solid and liquid phases. By contrast, at the elevated temperature, significant reductions in aqueous SO_4^{2-} concentrations occur in all experimental systems. The extent of this decline is inversely correlated with the pH, but it is positively correlated with the initial SO_4^{2-} concentration. These results demonstrate that elevated temperatures significantly promote the incorporation of SO_4^{2-} into solid phases, likely *via* enhanced mineral recrystallisation and structural substitution.[26] However, increasing the initial SO_4^{2-} concentration beyond 100 mM has minimal effect on the extent of concentration reduction, suggesting that the incorporation capacity of the transformation products is saturated. This observation can be attributed to the initial SO_4^{2-} levels substantially exceeding the incorporation capacity of the solid

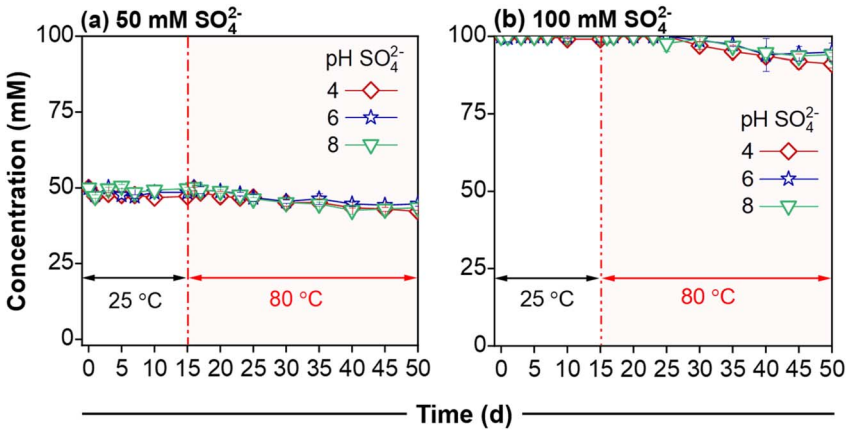

Fig. 1 Temporal changes in the aqueous SO_4^{2-} concentration during HFA transformation. These changes were investigated using various concentrations of SO_4^{2-} ((a) 50 mM and (b) 100 mM) at pH 4, 6, and 8.

phases. Overall, the results indicate that acidic conditions facilitate the incorporation process, possibly through the destabilization of HFA and ternary complex formation involving SO_4^{2-}, Fe(III), and As(V).[36]

To elucidate the impact of SO_4^{2-} on HFA stability and As(V) mobility, the aqueous concentrations of As(V) and Fe(III) were monitored simultaneously. The results shown in Fig. 2 reveal a marked pH-dependent behavior. Specifically, at pH 4, an increase in the SO_4^{2-} concentration significantly promotes As(V) release under both temperature conditions, whereas Fe(III) concentrations remain largely unchanged. This suggests that SO_4^{2-} facilitates As(V) mobilization *via* partial dissolution or anion substitution reactions without substantially altering the solubility of Fe(III) under acidic conditions.[26,37] By contrast, under circumneutral conditions (pH 6 and 8), SO_4^{2-} addition results in progressive declines in both As(V) and Fe(III) concentrations in the solution. These findings imply that SO_4^{2-} promotes the co-precipitation or stabilization of As(V) and Fe(III) in solid phases, potentially through the formation of basic ferric arsenate sulfate (BFAS) minerals or iron oxyhydroxysulfates, such as schwertmannite.[38,39] These observations demonstrate that the addition of SO_4^{2-} exerts a pronounced pH-dependent influence on As(V) mobility. Specifically, although an enhanced As(V) release is observed under acidic conditions,

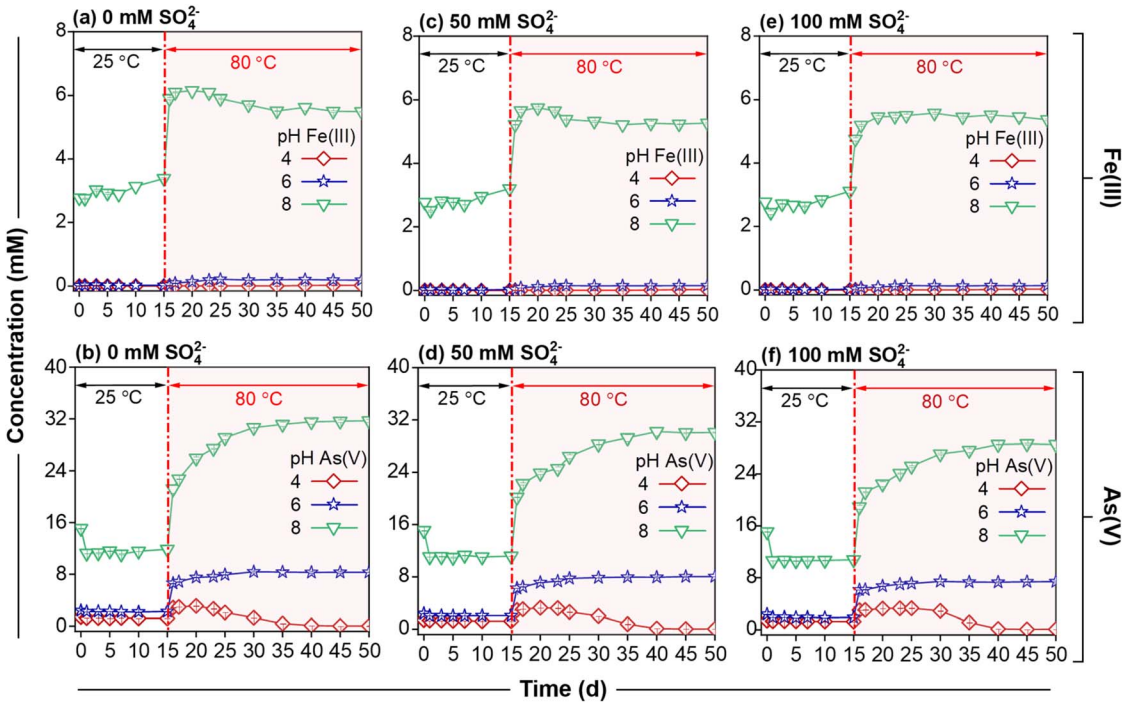

Fig. 2 Temporal changes in the concentrations of aqueous Fe(III) and As(V) during HFA transformation at SO_4^{2-} concentrations of (a and b) 0 mM, (c and d) 50 mM, and (e and f) 100 mM as a function of pH (4, 6, and 8) under the 25 °C condition for 15 d followed by aging at 80 °C (up to day 50).

As(v) solubility is suppressed under circumneutral pH conditions because of a greater degree of As(v) retention in the secondary Fe-bearing phases. These divergent behaviors underscore the importance of pH as a key variable in controlling the sulfate-mediated transformations of As(v)-bearing solids. At 25 °C, limited aqueous SO_4^{2-} reduction and pH-dependent Fe/As(v) partitioning are observed. By contrast, the temperature increase to 80 °C enhances the recrystallization-driven uptake and release—As(v) is sequestered at pH 4 during scorodite nucleation but rebounds at pH 6–8 owing to the thermal instability of the BFAS/schwertmannite-like phase.

3.2 XRD analysis

To track the mineralogical evolution of the current system during aging, the XRD patterns recorded for the sulfate-treated HFA (S-HFA) specimens were analyzed after 15 d at 25 °C and after subsequent aging at 80 °C (up to day 50) (Fig. 3). After 15 d at 25 °C, all samples exhibit two broad diffraction features centered at 2θ values of 29.63° and 58.70°, which are characteristic of amorphous phases. Minor peak shifts are observed across the examined pH range, which are attributed to incipient ferrihydrite formation, as evidenced by the slight diffraction shifts.[39] Notably, the presence of exogenous SO_4^{2-} (up to 100 mM) does not alter the amorphous natures of the solids under any of the investigated pH conditions, indicating that neither ambient aging nor SO_4^{2-} addition can solely induce any significant phase transformation during the initial 15 d. This result is consistent with the relatively stable aqueous Fe(III) and As(v) concentrations and minimal pH variations observed during these experiments.

By contrast, thermal treatment (80 °C, up to day 50) induces pronounced mineralogical changes, particularly at pH 4 (Fig. 3b). The formation of crystalline scorodite ($FeAsO_4 \cdot 2H_2O$, PDF #37-0468) is observed in all systems at pH 4, regardless of the initial SO_4^{2-} concentration. This transformation is corroborated by a sharp decline in the aqueous As(v) concentrations and the observation that the solid-phase Fe(III)/As(v) molar ratios approach unity (Table S2), which are consistent with the scorodite stoichiometry.[40–42] At pH 6 and 8, no distinct crystalline phases emerge under thermal conditions; only subtle peak shifts toward higher angles are detected, suggesting partial structural reorganization without complete mineral crystallization.

Overall, these findings indicate that elevated temperatures are a critical driver of scorodite crystallization under acidic conditions. However, at circumneutral pH values, prolonged heating and high sulfate concentrations fail to induce long-range structural ordering in the HFA-derived solids, likely because of the formation of metastable intermediate phases, such as ferrihydrite or BFAS.

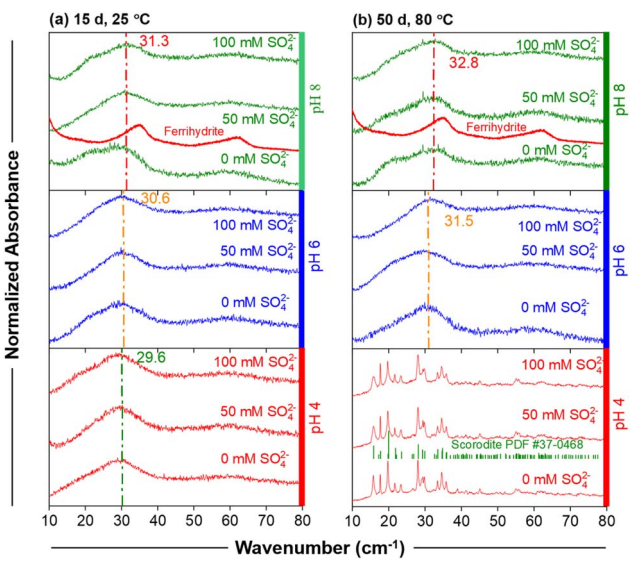

Fig. 3 XRD spectra recorded upon the addition of different concentrations of SO_4^{2-} to the HFA system on days 15 (a) and 50 (b) under different pH conditions.

3.3 FTIR spectroscopy

FTIR spectroscopy was used to track the structural evolution of the solid phases during HFA transformation in response to sulfate addition, wherein the spectra were collected at selected time points over a 50 d experimental period (Fig. 4). In the SO_4^{2-}-free system (Fig. 4a–c), significant structural changes are observed only at pH 4 under thermal treatment conditions. The emergence of distinct absorption bands at 813 cm^{-1} (ν_1 As–O stretching vibration) and at 2959 and 3515 cm^{-1} (ν_1 H–O stretching vibrations of the water molecules) confirms the formation of scorodite.[18,43,44] In addition, the peak observed at 869 cm^{-1}—commonly attributed to surface-bound arsenate species on ferrihydrite—exhibits a red-shift from 877 cm^{-1}, along with a narrowing full width at half maximum compared with the broader ν_1 As–O band observed for HFA (832 cm^{-1}); this further supports the transformation to a more ordered scorodite structure.[45] At circumneutral and mildly alkaline pH values (*i.e.*, 6 and 8, respectively), no diagnostic vibrational changes are observed, indicating that HFA remains largely amorphous under these conditions at both ambient and elevated temperatures.

Notably, the presence of sulfate markedly alters the FTIR spectral profiles, particularly under acidic and high-temperature conditions (Fig. 4d and e). Although scorodite eventually forms at pH 4 under all conditions, sulfate delays its crystallization.

More specifically, scorodite-specific bands appear by day 25 in the sulfate-free system; however, they are only clearly detected after days 30 and 40 in the 50 and 100 mM SO_4^{2-} systems, respectively. This delay is consistent with the slower declines in the aqueous As(v) concentrations and a lag in the pH recovery, indicating that sulfate interferes with the crystallization pathways, likely *via* anion competition or structural incorporation. At circumneutral and mildly alkaline pH values (6 and 8), the FTIR spectra show no clear evidence of scorodite formation (Fig. 4–i), in agreement with the XRD results. Instead, the early-stage samples (day 15) exhibit prominent sulfate bands at approximately 1136 cm^{-1} (ν_3 S–O) and 622 cm^{-1} (ν_4 S–O), consistent with the formation of BFAS-like phases.[46]

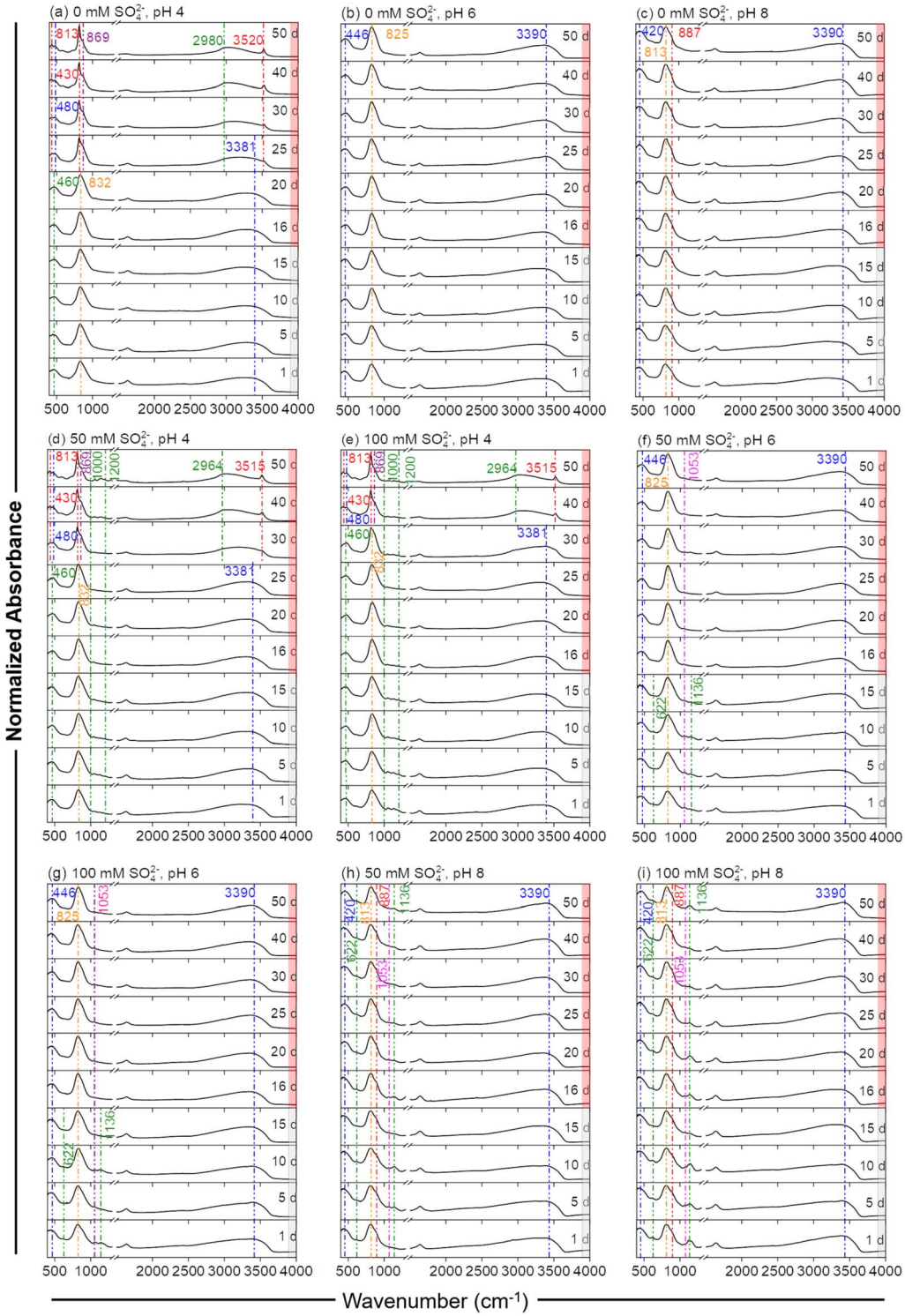

Fig. 4 FTIR spectra recorded upon the addition of different concentrations of SO_4^{2-} (a)–(c) 0 mM, (d), (f) and (h) 50 mM, and (e), (g) and (i) 100 mM to the HFA system at different pH conditions and over different stabilization times.

Additionally, the appearance of a peak at approximately 1053 cm^{-1} suggests the partial structural integration of sulfate into the HFA or BFAS matrices.[32] However, upon heating, these sulfate-related features weaken (pH 8) or disappear (pH 6), implying that the BFAS phases are metastable and prone to dissolution or transformation under thermal stress. Importantly, the persistence of elevated aqueous As(v) concentrations at pH 6–8 may inhibit further crystallization and stabilize the ferrihydrite-like intermediates.

Overall, these FTIR data underscore the role of sulfate as both a structural impurity and a kinetic inhibitor in arsenate mineral evolution, wherein it clearly exerts strong pH- and

temperature-dependent effects on the HFA transformation pathways.

3.4 Raman spectroscopy

Raman spectroscopy was employed to elucidate the structural evolution of SO_4^{2-}-treated HFA solids collected on days 15 and 30 (Fig. 5). The spectra of all samples exhibit the characteristic vibrational features of amorphous iron arsenates, including the symmetric stretching mode (ν_1) of AsO_4^{3-} at approximately 817 cm^{-1}, asymmetric stretching mode (ν_3) at approximately 876 cm^{-1}, and bending vibration (ν_2) of Fe–OH at approximately 470 cm^{-1}. These bands corroborate the presence of amorphous ferric arsenate species, consistent with the FTIR results.

Upon increasing the pH under ambient conditions, systematic shifts are observed in the Raman bands. Specifically, both the ν_1 and ν_3 As–O vibrations exhibit red shifts (*i.e.*, toward lower wavenumbers), whereas the ν_2 Fe–OH band shows a corresponding blue shift. These spectral changes likely reflect progressive alterations in the Fe/As(v) ratios and local bonding environments within the solid matrix, possibly due to minor structural rearrangements or early-stage phase separation.

Prolonged aging at 25 °C induces minimal phase transformations, as evidenced by the persistent broad, featureless bands characteristic of amorphous structures (Fig. 5a and b). By contrast, the addition of exogenous SO_4^{2-}, particularly under circumneutral conditions (pH 6 and 8), triggers the generation of a distinct Raman band at approximately 980 cm^{-1}. This band corresponds to the ν_1 symmetric stretching mode of the SO_4^{2-} component in schwertmannite, a poorly crystalline Fe(III) oxyhydroxysulfate. These observations indicate that SO_4^{2-} incorporation promotes schwertmannite-like phase formation under ambient temperature, consistent with the FTIR data.

Under the 80 °C condition, a pH-dependent divergence in the transformation behavior is observed. At pH 4, all samples exhibit spectral signatures consistent with the formation of crystalline scorodite, regardless of the SO_4^{2-} concentration.[47] This transformation is characterized by the sharpening and intensification of the As–O vibrational bands, indicating the presence of long-range structural ordering. By contrast, at pH 6, Raman features associated with schwertmannite (*i.e.*, at 980 cm^{-1}) disappear upon heating, suggesting its thermal instability and subsequent dissolution or transformation. Interestingly, at pH 8, the 980 cm^{-1} band persists, implying that schwertmannite exhibits greater stability under more mildly alkaline conditions.

Collectively, the Raman spectroscopy results reveal a complex interplay among the pH, SO_4^{2-} concentration, and temperature, which govern the structural evolution of HFA-derived solids. These findings support the proposed mechanism, wherein SO_4^{2-} not only modifies the phase composition through secondary mineral formation (*e.g.*, schwertmannite) but also influences the transformation kinetics and thermodynamic pathways under environmentally relevant conditions.

3.5 XPS analysis of the As(v) and Fe binding environments

XPS was conducted on the SO_4^{2-}-treated HFA solids collected on day 50 to elucidate the chemical environments of As(v) and Fe across varying pH conditions (Fig. 6). Specifically, the high-resolution spectra of the As $3d_{5/2}$ and Fe $2p_{3/2}$ components were deconvoluted to distinguish the binding modes under high sulfate loading conditions (100 mM) at pH 4, 6, and 8.

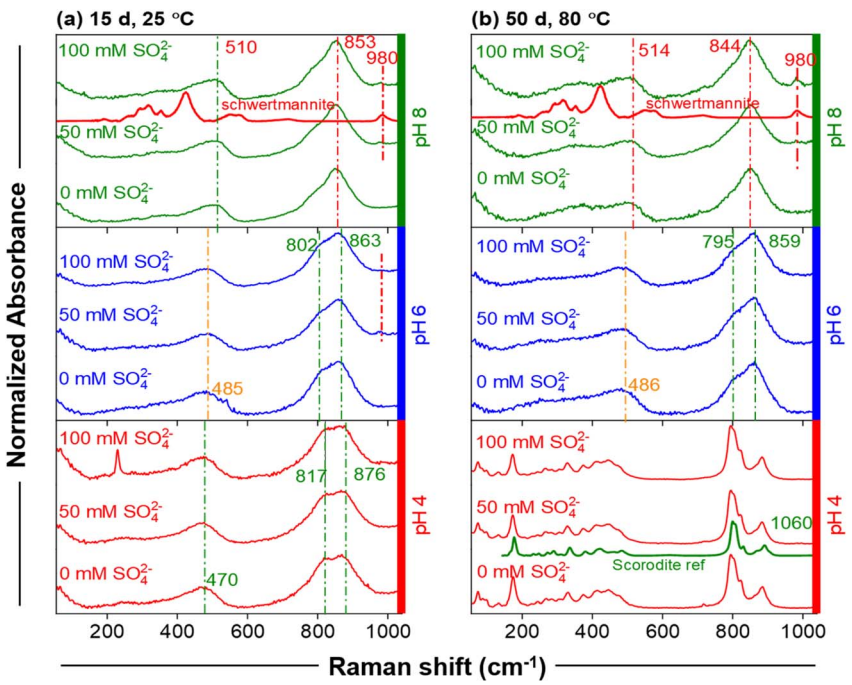

Fig. 5 Raman spectra recorded upon the addition of different concentrations of SO_4^{2-} to the HFA system on days (a) 15 and (b) 50 under different pH conditions.

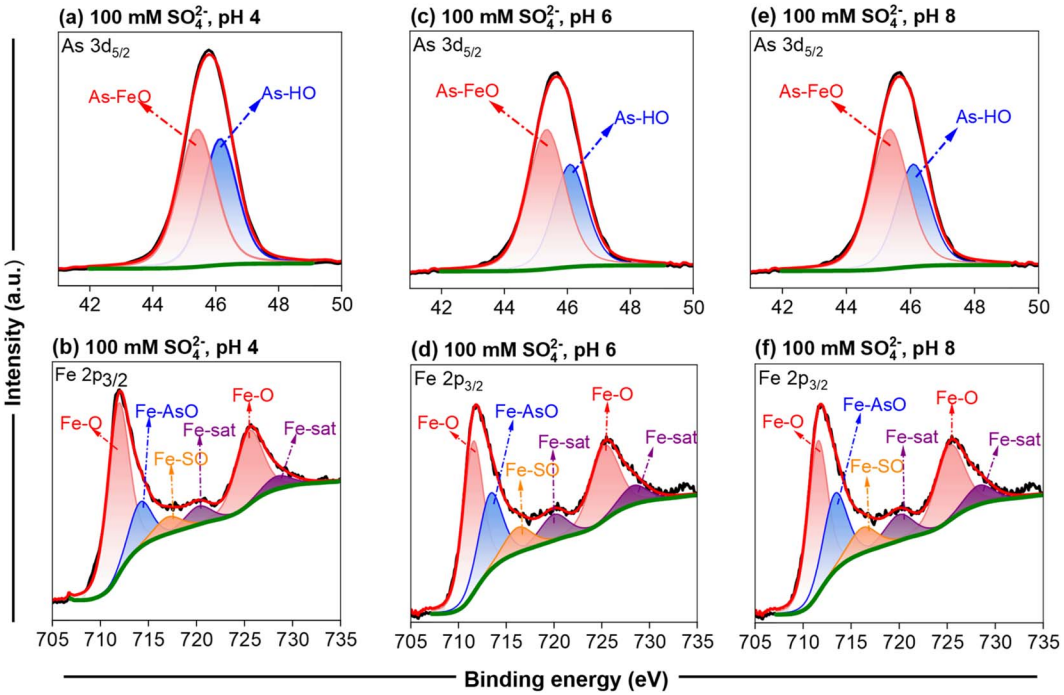

Fig. 6 XPS spectra collected for day 50, 80 °C, and after the addition of 100 mM SO_4^{2-} to the HFA under different pH conditions.((a and b) pH 4, (c and d) pH 6, and (e and f) pH 8).

The As $3d_{5/2}$ spectra recorded across all pH levels reveal consistent features centered at approximately 44.5–45.0 eV, attributable to As(v) species. Peak fitting resolves two primary components: one corresponding to Fe–AsO complexes (indicative of inner-sphere arsenate binding to ferric iron in scorodite or HFA) and the second associated with protonated arsenate species (*e.g.*, $HAsO_4^{2-}$, $H_2AsO_4^{-}$), suggesting the presence of hydrogen-bonded or surface-adsorbed As(v). The co-existence of these species implies a mixed arsenate coordination environment, which reflects the structural heterogeneity of the solid phase.

The Fe $2p_{3/2}$ spectra exhibit multiple splitting patterns characteristic of Fe(III), with binding energies centered at approximately 711.0–712.5 eV. Peak deconvolution identifies contributions from Fe–O (ferric hydroxides or ferrihydrite-like structures), Fe–As (scorodite or ferric arsenate frameworks), and Fe–SO bonds, which are indicative of sulfate incorporation into iron-bearing phases. The presence of Fe–SO suggests the formation of iron sulfate complexes or mixed iron arsenate–sulfate phases, such as BFAS.[48]

Importantly, these binding assignments align with the FTIR and Raman data (Fig. 4 and 5), confirming sulfate incorporation and structural reorganization within the solid matrix. The simultaneous detection of Fe–SO and As–FeO bonding environments across the pH conditions substantiates the hypothesis that sulfate modulates As(v) retention through ionic substitution, as well as promoting the stabilization of mixed-phase assemblages. Collectively, the XPS results provide direct molecular-scale evidence of pH- and sulfate-dependent coordination changes for both Fe and As(v), providing mechanistic insights into the competitive and cooperative interactions governing solid-phase As(v) sequestration in mining-affected systems.

3.6 Sulfate-mediated transformation mechanisms of HFA

The transformation behavior of HFA in sulfate-rich environments is governed by a complex interplay among ionic competition, structural substitution, and mineral solubility, with the pH and temperature acting as primary modulators. The strong chemical similarity between sulfate (SO_4^{2-}) and arsenate ($HAsO_4^{2-}$), particularly in terms of the charge, size, and Fe(III) affinity, allows sulfate to influence the HFA stability through three key pathways: (i) structural incorporation *via* isomorphic substitution with arsenate; (ii) Fe(III) complexation that promotes partial HFA dissolution; (iii) inhibition of recrystallisation by disrupting lattice reordering during phase transitions.

Under circumneutral to mildly alkaline conditions (pH 6–8), HFA undergoes incongruent dissolution into ferrihydrite, a metastable Fe(III) oxyhydroxide. In this system, the co-existing sulfate facilitates the subsequent formation of BFAS or schwertmannite-like phases through ternary co-precipitation with Fe(III) and As(v). Although these intermediate phases serve as transient sinks for As(v), they are thermally unstable. Upon heating, the BFAS phases dissolve, releasing arsenate back into the solution or transforming into less-crystalline Fe phases. Therefore, the long-term immobilization capacities of BFAS phases are limited under fluctuating geochemical conditions. Both BFAS and schwertmannite are metastable and susceptible to dissolution or transformation in response to thermal or redox/pH fluctuations, which constrains their ability to retain As(v) over extended periods. By contrast, scorodite is well-crystalline and exhibits low solubility under acidic conditions. Although SO_4^{2-} initially inhibits its nucleation, it is ultimately excluded from the crystalline structure, resulting in the formation of a stable terminal sink for As.

Conversely, under acidic and thermally elevated conditions (*e.g.*, pH 4, 80 °C), HFA transformation is dominated by recrystallisation into scorodite. Although sulfate incorporation initially inhibits nucleation and retards the transformation kinetics, crystalline scorodite forms over time. This transformation is facilitated by a progressive increase in the supersaturation of dissolved Fe(III) and As(V), which promotes scorodite precipitation. However, the structurally incorporated sulfate is ultimately excluded during scorodite crystallization because of its incompatibility with the scorodite lattice, which increases the energy barrier for mineral ordering and reduces the overall crystallization rate.

3.7 Mechanisms of As(V) and Fe redistribution

Sulfate addition triggers a significant redistribution of As(V) and Fe(III) between the aqueous and solid phases, which is governed by a combination of ligand exchange, dissolution–reprecipitation, and phase transformation mechanisms. At a low pH, sulfate enhances the mobilization of As(V) *via* two processes, namely competitive substitution for As(V) within the HFA structure, leading to As(V) release, and Fe(III)–SO_4^{2-} complexation at the HFA surface (eqn (1)), which promotes Fe dissolution and destabilizes the solid phase.

$$Fe^{3+}\text{–}HAsO_4^{2-} + SO_4^{2-} \rightarrow Fe^{3+}\text{–}SO_4^{2-} + HAsO_4^{2-} \quad (1)$$

By contrast, at pH 6 and 8, the addition of SO_4^{2-} immobilizes both As(V) and Fe(III) by promoting the formation of mixed-phase BFAS minerals (eqn (2)). However, these phases are sensitive to thermal destabilization, as described above. Notably, the high As(V) concentrations observed in heated mildly alkaline systems suggest that the breakdown of BFAS phases releases previously immobilized As(V) while simultaneously hindering further transformation to more stable phases, such as scorodite. These results emphasize the metastable nature of BFAS and limited robustness of sulfate-driven immobilization under non-isothermal conditions.

$$Fe^{3+} + (1-x)AsO_4^{3-} + xSO_4^{2-} + xOH^- \rightarrow Fe(AsO_4)_{1-x}(SO_4)_x(OH)_x \quad (2)$$

Thermal dissolution of HFA supports these observations. More specifically, as outlined in eqn (3), heating initiates HFA breakdown, releasing $H_2AsO_4^-$, Fe(III), and protons, which lower the system pH. The subsequent addition of NaOH to maintain the pH enhances ferrihydrite formation, whereas As(V)-induced Fe(III) dissolution (eqn (4)) and reprecipitation create favorable conditions for scorodite nucleation. Nonetheless, the presence of sulfate suppresses this crystallization process through impurity exclusion and lattice disruption because it competes with As(V) for Fe(III) coordination during recrystallisation.

$$FeAsO_4\cdot xH_2O(HFA) + 3H_2O \rightarrow Fe(OH)_3 + H_2AsO_4^- + (x-3)H_2O + H^+ \quad (3)$$

$$Fe(OH)_3 \rightarrow Fe^{3+} + 3OH^- \quad (4)$$

3.8 Environmental implications

These findings highlight the importance of considering both pH and temperature fluctuation when predicting the fate of As(V) in sulfate-rich environments. The behavior of SO_4^{2-} differs substantially under acidic *vs.* circumneutral conditions, significantly influencing the mobility of As(V) in mining-affected environments. In acidic tailings or AMD systems, SO_4^{2-} promotes As(V) release and delays its transformation into stable phases, thereby increasing the As(V) bioavailability. On the contrary, in neutralized or passively treated systems, SO_4^{2-} enhances short-term As(V) retention through BFAS formation; however, this retention is susceptible to breakdown during warming or drying–rewetting cycles. Consequently, remediation strategies should, therefore, prioritize pH control and consider SO_4^{2-} levels to minimize re-mobilization. This work enables more accurate prediction of As(V) behavior in sulfate-laden environments and supports the development of tailored stabilization approaches for long-term mitigation. From a management perspective, SO_4^{2-} concentration near the U.S. EPA's Secondary Maximum Contaminant Level (SMCL 250 mg L^{-1}) and those commonly found in AMD settings highlight the need to co-manage pH, temperature, and sulfate fluxes when choosing between short-term BFAS-based retention and the promotion of scorodite as a durable sink. This work enables more accurate prediction of As(V) behavior in sulfate-laden environments and supports the development of tailored stabilization strategies for long-term mitigation.

Nevertheless, this study faced several challenges inherent to investigating amorphous-to-crystalline phase transformations. The primary limitation was the definitive identification of the initial HFA and its transient intermediates. Although we employed a combination of techniques (XRD, FTIR, Raman, and XPS) to infer chemical composition and morphological changes, the precise molecular structure of these amorphous phases remains uncertain. Additionally, the experimental conditions, though designed to simulate accelerated aging, may not fully represent longer-term natural processes. The use of elevated temperature (80 °C) to induce transformation over a 35 d period assumes analogous pathways to slower ambient processes, which may not capture all potential intermediate phases or kinetics.

4. Conclusions

This study investigated the transformation behavior of amorphous HFA mediated by sulfate anions (SO_4^{2-}) under surface-generated oxidation conditions to elucidate the geochemical cycling of As(V), Fe, and S in sulfate-rich systems. It was revealed that although SO_4^{2-} promoted As(V)/Fe release from solids at pH 4, it inhibited the release at pH 6 and 8. Additionally, SO_4^{2-} incorporated into solids across all pH conditions, with elevated temperatures and high SO_4^{2-} concentrations enhancing its structural incorporation. More specifically, while SO_4^{2-} was incorporated into HFA/scorodite at pH 4, it generated BFAS at pH 6 and 8. Furthermore, at pH 4 and heating to 80 °C, HFA was fully transformed to crystalline scorodite despite the SO_4^{2-}-

induced inhabitation of crystallization. By contrast, the BFAS formed at 25 °C and pH 6 and 8 dissolved upon heating. These findings demonstrate that SO_4^{2-} critically regulates the mobility of As(v) through pH-dependent mechanisms. Thus, acidic conditions facilitate dissolution–complexation pathways(*i.e.*, SO_4^{2-}–Fe(III)/As(v)–Fe(III) complexation and anion substitution), whereas neutral to mildly alkaline conditions promote immobilization *via* BFAS formation.

Author contributions

Xuedi Wang: writing – original draft, data curation. Rui Su: funding acquisition. Miao Xu: investigation. Yuyin Ma: investigation. Yanjiao Gao: supervision. Xu Ma: funding acquisition, project administration, supervision.

Conflicts of interest

There are no conflicts to declare.

Data availability

The author confirms that the data supporting the finding of this study are available within the article and the supplementary information (SI). Supplementary information: solid characterization method and other solid–liquid phase analysis data during the experiment. See DOI: **https://doi.org/10.1039/d5ra05160f**.

Acknowledgements

We thank the National Natural Science Foundation of China (No. 42207258), the Liaoning Provincial Natural Science Foundation Program Project (No. 2024-MSLH-2000 and 2024JH2/102600103), Liaoning Provincial Department of Education Basic Research Program for Colleges and Universities (No. JYTMS20230857) and Fundamental Research Funds for the Central Universities (No. 044420250070) for financial support.

Notes and references

1 R. Kaur, A. Garkal, L. Sarode, P. Bangar, T. Mehta, D. P. Singh and R. Rawal, Understanding arsenic toxicity: Implications for environmental exposure and human health, *J. Hazard. Mater. Lett.*, 2024, **5**, 100090.

2 H. X. Qiu, X. H. Sun, B. Z. Wu, X. Q. Su and M. Z. Hu, Mechanism of arsenic release process from arsenopyrite chemical oxidation, *Sci. Total Environ.*, 2024, **915**, 169969.

3 D. Langmuir, J. Mahoney, A. MacDonald and J. Rowson, Predicting arsenic concentrations in the porewaters of buried uranium mill tailings, *Geochim. Cosmochim. Acta*, 1999, **63**, 3379–3394.

4 J. Majzlan, B. Lalinská, M. Chovan, L. Jurkovič, S. Milovská and J. Göttlicher, The formation, structure, and ageing of As-rich hydrous ferric oxide at the abandoned Sb deposit Pezinok (Slovakia), *Geochim. Cosmochim. Acta*, 2007, **71**, 4206–4220.

5 D. Paktunc, A. Foster, S. Heald and G. Laflamme, Speciation and characterization of arsenic in gold ores and cyanidation tailings using X-ray absorption spectroscopy, *Geochim. Cosmochim. Acta*, 2004, **68**, 969–983.

6 W. P. Inskeep, R. E. Macur, G. Harrison, B. C. Bostick and S. Fendorf, Biomineralization of As(V)-hydrous ferric oxyhydroxide in microbial mats of an acid-sulfate-chloride geothermal spring, Yellowstone National Park, *Geochim. Cosmochim. Acta*, 2004, **68**, 3141–3155.

7 E. D. Burton, R. T. Bush and L. A. Sullivan, Sedimentary iron cycling in waterways associated with acid sulfate soils, *Geochim. Cosmochim. Acta*, 2006, **70**, A76.

8 E. D. Burton, R. T. Bush and L. A. Sullivan, Sedimentary iron geochemistry in acidic waterways associated with coastal lowland acid sulfate soils, *Geochim. Cosmochim. Acta*, 2006, **70**, 5455–5468.

9 D. Langmuir, J. Mahoney and J. Rowson, Solubility products of amorphous ferric arsenate and crystalline scorodite ($FeAsO_4 \cdot 2H_2O$) and their application to arsenic behavior in buried mine tailings, *Geochim. Cosmochim. Acta*, 2006, **70**, 2942–2956.

10 F. Maillot, G. Morin, F. Juillot, O. Bruneel, C. Casiot, G. Ona-Nguema, Y. Wang, S. Lebrun, E. Aubry, G. Vlaic and G. E. Brown, Structure and reactivity of As(III)-and As(V)-rich schwertmannites and amorphous ferric arsenate sulfate from the Carnoulès acid mine drainage, France: Comparison with biotic and abiotic model compounds and implications for As remediation, *Geochim. Cosmochim. Acta*, 2013, **104**, 310–329.

11 P. L. Smedley and D. G. Kinniburgh, A review of the source, behaviour and distribution of arsenic in natural waters, *Appl. Geochem.*, 2002, **17**, 517–568.

12 J. Wright, E. Cathcart, S. Walther and B. O'Shea, Role of climate and geography in arsenic mobility and risk at an artisanal mining site in an urbanized semi-arid environment, *J. Environ. Manage.*, 2022, **304**, 114163.

13 X. L. An, F. G. Huang, H. T. Ren, Y. F. Wang, Y. Chen, Z. M. Liu, H. W. Zhang and X. Han, Oxidative dissolution of amorphous FeS and speciation of secondary Fe minerals: Effects of pH and As(III) concentration, *Chem. Geol.*, 2017, **462**, 44–54.

14 S. Hu, F. Q. Lian and J. F. Wang, Effect of pH to the surface precipitation mechanisms of arsenate and cadmium on TiO_2, *Sci. Total Environ.*, 2019, **666**, 956–963.

15 H. H. Du, N. Nie, W. K. Rao, L. Lu, M. Lei and B. Q. Tie, Ferrihydrite–organo composites are a suitable analog for predicting Cd(II)–As(V) coexistence behaviors at the soil solid-liquid interfaces, *Environ. Pollut.*, 2021, **290**, 118040.

16 Z. Chen, S. P. Geng, J. Xiao, F. Y. Zhao, K. Wang, Y. Wang, P. Tsiakaras and S. Q. Song, Understanding the selectivity trend of water and sulfate (SO_4^{2-}) oxidation on metal oxides: On-site synthesis of persulfate, H_2O_2 for wastewater treatment, *Chem. Eng. J.*, 2022, **431**, 134332.

17 Y. F. Jia and G. P. Demopoulos, Coprecipitation of arsenate with iron(III) in aqueous sulfate media: Effect of time, lime as base and co-ions on arsenic retention, *Water Res.*, 2008, **42**, 661–668.

18 S. F. Wang, X. Ma, G. Q. Zhang, Y. F. Jia and K. Hatada, New Insight into the Local Structure of Hydrous Ferric Arsenate Using Full-Potential Multiple Scattering Analysis, Density Functional Theory Calculations, and Vibrational Spectroscopy, *Environ. Sci. Technol.*, 2016, **50**, 12114–12121.

19 D. G. Rancourt, D. Fortin, T. Pichler, P.-J. Thibault, G. Lamarche, R. V. Morris and P. H. J. Mercier, Mineralogy of a natural As-rich hydrous ferric oxide coprecipitate formed by mixing of hydrothermal fluid and seawater: Implications regarding surface complexation and color banding in ferrihydrite deposits, *Am. Mineral.*, 2001, **86**, 834–851.

20 L. Carlson, J. M. Bigham, U. Schwertmann, A. Kyek and F. Wagner, Scavenging of As from acid mine drainage by schwertmannite and ferrihydrite: a comparison with synthetic analogues, *Environ. Sci. Technol.*, 2002, **36**, 1712–1719.

21 M. A. Inam, R. Khan, K. H. Lee, M. Akram, Z. Ahmed, K. G. Lee and Y. M. Wie, Adsorption Capacities of Iron Hydroxide for Arsenate and Arsenite Removal from Water by Chemical Coagulation: Kinetics, Thermodynamics and Equilibrium Studies, *Molecules*, 2021, **26**, 7046.

22 D. W. Cai, S. Q. Kong, Y. X. Shao, J. J. Liu, R. Q. Liu, X. G. Wei, B. Bai, D. Werner, X. B. Gao and C. C. Li, Mobilization of arsenic from As-containing iron minerals under irrigation: Effects of exogenous substances, redox condition, and intermittent flow, *J. Hazard. Mater.*, 2022, **440**, 129736.

23 A. M. Nazari, R. Radzinski and A. Ghahreman, Review of arsenic metallurgy: Treatment of arsenical minerals and the immobilization of arsenic, *Hydrometallurgy*, 2017, **174**, 258–281.

24 D. Paktunc and K. Bruggeman, Solubility of nanocrystalline scorodite and amorphous ferric arsenate: Implications for stabilization of arsenic in mine wastes, *Appl. Geochem.*, 2010, **25**, 674–683.

25 E. Krause and V. A. Ettel, Solubilities and stabilities of ferric arsenate compounds, *Hydrometallurgy*, 1989, **22**, 311–337.

26 X. Ma, R. Su, X. M. Zhao, S. J. Liu, X. Wu, S. F. Wang and Y. F. Jia, Phase transformation of hydrous ferric arsenate in the presence of Fe(II) under anaerobic conditions: Implications for arsenic mobility and fate in natural and anthropogenic environments, *Chem. Geol.*, 2021, **578**, 120321.

27 Z. H. Rong, X. C. Tang, L. P. Wu, X. Chen, W. Dang, X. Li, L. C. Huang and Y. Wang, The effect of precursor speciation on the growth of scorodite in an atmospheric scorodite synthesis, *R. Soc. Open Sci.*, 2020, **7**, 191619.

28 N. Papassiopi, E. Virčiková, V. Nenov, A. Kontopoulos and L. Molnár, Removal and fixation of arsenic in the form of ferric arsenates. Three parallel experimental studies, *Hydrometallurgy*, 1996, **41**, 243–253.

29 M. Filippi, V. Goliáš and Z. Pertold, Arsenic in contaminated soils and anthropogenic deposits at the Mokrsko, Roudný, and Kašperské Hory gold deposits, Bohemian Massif (CZ), *Environ. Geol.*, 2004, **45**, 716–730.

30 X. Ma, Z. D. Yuan, M. A. Gomez, X. Wang, S. F. Wang, S. H. Yao and Y. F. Jia, A qualitative and quantitative investigation of partitioning and local structure of arsenate in barite lattice during coprecipitation of barium, sulfate, and arsenate, *Am. Mineral.*, 2017, **102**, 2512–2520.

31 X. Ma, S. H. Yao, Z. D. Yuan, R. Bi, X. Wu, J. X. Zhang, S. F. Wang, X. Wang and Y. F. Jia, Detoxification and reclamation of hydrometallurgical arsenic- and trace metals-bearing gypsum via hydrothermal recrystallization in acid solution, *Chemosphere*, 2020, **250**, 126290.

32 X. Ma, S. F. Wang, M. A. Gomez, Z. D. Yuan, X. Wu, S. H. Yao and Y. F. Jia, Insight into the effect of SO_4^{2-} on the precipitation and solubility of ferric arsenate in acidic solutions: Implication for arsenic mobility and fate, *Chem. Geol.*, 2022, **602**, 120900.

33 X. Ma, Z. D. Yuan, J. R. Lin, Y. B. Cui, S. F. Wang, Y. M. Pan, R. Chernikov, L. K. L. Cheung, R. Deevsalar and Y. F. Jia, Local Structure and Crystallization Transformation of Hydrous Ferric Arsenate in Acidic H_2O–Fe(III)–As(V)–SO_4^{2-} Systems: Implications for Acid Mine Drainage and Arsenic Geochemical Cycling, *Environ. Sci. Technol.*, 2024, **58**, 7176–7185.

34 J. A. Grande, A. Jiménez, S. Romero, M. L. D. L. Torre and T. G. Olivera, Quantification of Heavy Metals from A.M.D. Dischargedinto a Public Water Supply Dam in the Iberian Pyrite Belt (SW Spain) Using Centered Moving Average, *Water. Air. Soil Pollut.*, 2010, **212**, 299–307.

35 M. Neal, C. Neal, H. Wickham and S. Harman, Determination of bromide, chloride, fluoride, nitrate and sulphate by ion chromatography: comparisons of methodologies for rainfall, cloud water and river waters at the Plynlimon catchments of mid-Wales, *Hydrol. Earth Syst. Sci.*, 2007, **11**, 294–300.

36 M. A. Gomez, G. Ventruti, M. Celikin, H. Assaaoudi, H. Putz, L. Becze, K. E. Lee and G. P. Demopoulos, The nature of synthetic basic ferric arsenate sulfate ($Fe(AsO_4)_{1-x}(SO_4)_x(OH)_x$) and basic ferric sulfate ($FeOHSO_4$): their crystallographic, molecular and electronic structure with applications in the environment and energy, *RSC Adv.*, 2013, **3**, 16840.

37 J. Majzlan and S. C. B. Myneni, Speciation of Iron and Sulfate in Acid Waters: Aqueous Clusters to Mineral Precipitates, *Environ. Sci. Technol.*, 2005, **39**, 188–194.

38 Z. Q. Zhu, H. Q. Yang, J. Liu, Y. N. Zhu, S. Tang, L. H. Zhang and X. X. Wang, Dissolution, Solubility, and Stability of the Basic Ferric Sulfate Arsenates $[Fe(SO_4)_x(AsO_4)_y(OH)_z \cdot nH_2O]$ at 25–45°C and pH 2–10, *J. Chem.*, 2021, **2021**, 1–14.

39 S. Paikaray, Environmental Stability of Schwertmannite: A Review, *Mine Water Environ.*, 2021, **40**, 570–586.

40 T. Fujita, R. Taguchi, M. Abumiya, M. Matsumoto, E. Shibata and T. Nakamura, Effects of zinc, copper and sodium ions on ferric arsenate precipitation in a novel atmospheric scorodite process, *Hydrometallurgy*, 2008, **93**, 30–38.

41 T. Fujita, R. Taguchi, M. Abumiya, M. Matsumoto, E. Shibata and T. Nakamura, Effect of pH on atmospheric scorodite synthesis by oxidation of ferrous ions: Physical properties and stability of the scorodite, *Hydrometallurgy*, 2009, **96**, 189–198.

42 T. Fujita, S. Fujieda, K. Shinoda and S. Suzuki, Environmental leaching characteristics of scorodite synthesized with Fe(II) ions, *Hydrometallurgy*, 2012, **111–112**, 87–102.

43 R. Su, X. Ma, X. L. Yin, X. M. Zhao, Z. D. Yan, J. R. Lin, X. F. Zeng, D. N. Zhang, S. F. Wang and Y. F. Jia, Arsenic removal from hydrometallurgical waste sulfuric acid via scorodite formation using siderite ($FeCO_3$), *Chem. Eng. J.*, 2021, **424**, 130552.

44 G. Y. Cai, X. Zhu, K. Z. Li, X. J. Qi, Y. G. Wei, H. Wang and F. Y. Hao, Self-enhanced and efficient removal of arsenic from waste acid using magnetite as an in situ iron donator, *Water Res.*, 2019, **157**, 269–280.

45 M. A. Gomez, L. Becze, J. N. Cutler and G. P. Demopoulos, Hydrothermal reaction chemistry and characterization of ferric arsenate phases precipitated from $Fe_2(SO_4)_3$–As_2O_5–H_2SO_4 solutions, *Hydrometallurgy*, 2011, **107**, 74–90.

46 M. A. Gomez, H. Assaaoudi, L. Becze, J. N. Cutler and G. P. Demopoulos, Vibrational spectroscopy study of hydrothermally produced scorodite ($FeAsO_4 \cdot 2H_2O$), ferric arsenate sub-hydrate (FAsH; $FeAsO_4 \cdot 0.75H_2O$) and basic ferric arsenate sulfate (BFAS; $Fe[(AsO_4)_{1-x}(SO_4)_x(OH)_x] \cdot wH_2O$), *J. Raman Spectrosc.*, 2010, **41**, 212–221.

47 R. L. Frost, R. Scholz, J. Jirásek and F. M. Belotti, An SEM–EDX and Raman spectroscopic study of the fibrous arsenate mineral liskeardite and in comparison with other arsenates kaňkite, scorodite and yvonite, *Spectrochim. Acta, Part A*, 2015, **151**, 566–575.

48 J. T. Kloprogge and B. J. Wood, X-ray Photoelectron Spectroscopic and Raman microscopic investigation of the variscite group minerals: Variscite, strengite, scorodite and mansfieldite, *Spectrochim. Acta, Part A*, 2017, **185**, 163–172.